Power Electronic Systems
Laboratory

IEEE Transaction on Magnetics, Vol. 47, No. 5, pp. 910-913, May 2011.

An Extension of PEEC Method for Magnetic Materials Modeling in Frequency Domain

I. Kovacevic
A. Müsing
J. W. Kolar

Eidgenössische Technische Hochschule Zürich
Swiss Federal Institute of Technology Zurich

An Extension of PEEC Method for Magnetic Materials Modeling in Frequency Domain

Ivana Ferdinand Kovačević, Andreas M. Müsing, and Johann Walter Kolar

Power Electronic Systems Laboratory, ETH Zurich, CH-8092 Zurich, Switzerland

An extension of the partial element equivalent circuit (PEEC) method for magnetic materials modeling in the frequency domain applied on toroidal magnetic inductors with rectangular cross section is presented in this paper. The extension is performed by coupling the PEEC method and the boundary element method (BEM). The influence of magnetic material is modeled by distributions of "fictitious magnetic currents and charges" existing on the surface of a magnetic body. To verify the developed 3-D PEEC model, calculated and measured impedances are compared for two winding arrangements employing a ferrite T38 core. A good agreement between the PEEC simulation and measurements is presented up to the first resonant frequency. The described PEEC modeling approach enables 3-D electromagnetic simulations with much less computational effort than given for existing finite element method (FEM) simulators.

***Index Terms*—Boundary element method (BEM), fictitious magnetic currents and charges, partial element equivalent circuit (PEEC), toroidal magnetic inductors.**

I. Introduction

AS ELECTRONIC devices must comply with electromagnetic compatibility (EMC) standards, a comprehensive knowledge of their high-frequency electromagnetic behavior is of great importance. Accordingly, there is a need for virtual prototyping and a fast EM simulator applicable for various electromagnetic interference (EMI) problems. EMI simulation is based on accurate modeling of all parasitic EM coupling effects, and the partial element electric circuit (PEEC) method has shown to be a convenient modeling approach.

The PEEC approach is a well-suitable method for numerical simulation of the EM field problems coupled to electrical circuits such as EMI filters, power converters, printed circuit boards (PCBs), etc. The PEEC method is based on the integral formulation of Maxwell's equations and their interpretation in terms of partial circuit elements both in time and frequency domain. So far, several extensions were added to the standard PEEC method, e.g., modeling in the presence of dielectrics and a PEEC solver for nonorthogonal geometries [1]. However, PEEC models of magnetic components (transformers, inductors, etc.) are missing as there is a difficulty to apply the PEEC approach in the presence of nonlinear and nonhomogenously magnetized materials. Therefore, an extension to the standard PEEC method is presented in this paper on the example of a toroidal inductor with rectangular cross section. Due to their geometrical characteristics and magnetic properties, toroidal inductors are frequently used, and considerable effort is made to accurately model their behavior in a wide frequency range.

PEEC modeling in the presence of magnetic materials has been investigated recently in several publications [2]–[6]. The PEEC approach for linear magnetic materials was solved in [2]–[4] by replacing a magnetized object with an equivalent distribution of magnetic currents and then writing the correlation matrices between induced electric and fictitious magnetic currents. However, PEEC modeling of magnetic components was not considered. A PEEC-based modeling method of common mode (CM) inductors assuming that the direction of stray field is not significantly influenced by the ferromagnetic core was proposed in [5]. This approach does not take into account the 3-D structure of the coil, and it is not applicable for an arbitrary-shaped magnetic geometry. By the hybrid FEM-PEEC coupled method in [6], the problem of a complex FEM mesh is not fully avoided, but is lessened in the way that the mesh around conductors is relaxed.

Manuscript received May 21, 2010; accepted August 23, 2010. Date of current version April 22, 2011. Corresponding author: I. F. Kovačević (e-mail: kovacevic@lem.ee.ethz.ch).

Color versions of one or more of the figures in this paper are available online at http://ieeexplore.ieee.org.

Digital Object Identifier 10.1109/TMAG.2010.2073449

II. Magnetic Current and Charge Approach

The EM influence of a magnetized object is fully described by the magnetization vector $\mathbf{M}$ defined within the magnetic volume. $\mathbf{M}$ influences the magnetic field produced by surrounding field sources, and the introduced change can be modeled by the magnetic vector potential $\mathbf{A_M}$ or the magnetic scalar potential $V^{(M)}$ [7]. Using magnetic potentials, it can be shown that the influence of magnetization $\mathbf{M}$ in the volume V_m on the total magnetic field at any point in space is equivalent to the influence of a volume and surface "fictitious magnetic current" $(\mathbf{J_M}, \mathbf{K_M})$ and "fictitious magnetic charge" (ρ_M, σ_M) distribution in free-space μ_0 existing within the volume V_m and/or onto its surface S_m

$$\mathbf{B_M}(\mathbf{r}) = \frac{\mu_0}{4\pi}\int\limits_{V_m} \frac{\mathbf{J_M}(\mathbf{r_m})\times(\mathbf{r}-\mathbf{r_m})}{|\mathbf{r}-\mathbf{r_m}|^3}\mathrm{d}V_m + \frac{\mu_0}{4\pi}\oint\limits_{S_m} \frac{\mathbf{K_M}(\mathbf{r_m})\times(\mathbf{r}-\mathbf{r_m})}{|\mathbf{r}-\mathbf{r_m}|^3}\mathrm{d}S_m \quad (1)$$

$$\mathbf{J_M} = \nabla_{\mathbf{r_m}} \times \mathbf{M}(\mathbf{r_m}), \quad \mathbf{K_M} = \mathbf{M}(\mathbf{r_m}) \times \mathbf{n}(\mathbf{r_m}) \quad (2)$$

$$\mathbf{H_M}(\mathbf{r}) = \frac{1}{4\pi}\int\limits_{V_m} \frac{\rho_M(\mathbf{r_m})(\mathbf{r}-\mathbf{r_m})}{|\mathbf{r}-\mathbf{r_m}|^3}\mathrm{d}V_m + \frac{1}{4\pi}\oint\limits_{S_m} \frac{\sigma_M(\mathbf{r_m})(\mathbf{r}-\mathbf{r_m})}{|\mathbf{r}-\mathbf{r_m}|^3}\mathrm{d}S_m \quad (3)$$

$$\rho_m(\mathbf{r_m}) = -\nabla_{\mathbf{r_m}} \cdot \mathbf{M}(\mathbf{r_m}), \sigma_m(\mathbf{r_m}) = \mathbf{M}(\mathbf{r_m}) \cdot \mathbf{n}(\mathbf{r_m}). \quad (4)$$

The currents $\mathbf{J_M}$ and $\mathbf{K_M}$ are bounded fictitious volume and surface currents known as "Amperian" currents that influence the magnetic field, but do not generate a voltage drop along

the magnetic volume or its surface. The magnetic charges contribute to the total magnetic field with $\mathbf{H_M}$. The typically used magnetic cores—i.e., powder, ferrite, iron, and amorphous cores—are characterized by their effective relative permeability μ_r (the permeability of a homogeneous core with the same characteristics as the actual composite core material). Accordingly, magnetic cores are assumed to be linear and homogeneous isotropic magnetic circuits so that the first terms of (1) and (3) are zero, i.e., the magnetic volume does not have to be discretized.

A. Magnetic Core Properties

A linear magnetic core is described by the permeability μ_r or magnetic susceptibility $\chi_\mathrm{m} = \mu_\mathrm{r} - 1$. As the real behavior of magnetic materials varies with frequency f and magnetic field H, μ_r is not constant, but defined as a function of these variables: $\mu_\mathrm{r} = \mu_\mathrm{r}(f, H)$. Core manufacturers typically provide either the effective relative permeability μ_r or the complex permeability μ' and μ'', i.e., $\underline{\mu} = \mu' - \mathrm{j}\mu''$ versus frequency characteristics. In conventional complex permeability measurements, the real μ' and imaginary μ'' components are recalculated from the measured total impedance Z_L assuming that the inductor can be represented by a series resistance R_S and a series inductance L_S. Accordingly, the real part μ' describes an increase of inductance compared to an air-core inductor, whereas the imaginary part μ'' defines the losses and the phase shift between the magnetic field and the flux within core. As the winding arrangement and the dielectric core properties can also take influence on the total impedance of an inductor, the accuracy of complex permeability curves extracted from the total impedance can be disputable. For higher frequencies, more accurate specification of the permeability curves is required.

In the first modeling stage, the permeability dependency $\mu_\mathrm{r}(f)$ is used. Further investigation of the nonlinear behavior of core material described by $B - H$ hysteresis characteristic will be conducted in future research. In the applications where dc-bias changes in time, i.e., the operating point moves along the $B - H$ curve, the permeability varies in time and $\mu_\mathrm{r} = \mu_\mathrm{r}(H)$ needs to be considered. Modeling of nonlinear core characteristics in the frequency domain becomes difficult, and a time-domain model appears more convenient, but then the modeling problem of core losses defined by $\underline{\mu}$ arises.

B. Magnetic Core Surface Currents and Charges

The physical interpretation of virtual magnetic currents and charges can be obtained from (2) and (4): Virtual magnetic charges are equal to the component of magnetization vector $\mathbf{M}$ normal to the surface S_m, i.e., the stray field, while the magnetic field lines tangential to the main magnetic path of the core can be modeled only by means of the virtual magnetic currents. A toroidal coil with its windings equally distributed over the entire core surface has a very low magnetic stray field, and the magnetic field lines are almost tangential to the magnetic path. This means that, in an ideal case, no magnetic charge exists. Therefore, with only the magnetic charge approach, the flux lines and inductance enhancement due to the presence of the magnetic core cannot be modeled.

The magnetic surface currents $\mathbf{K_M}$ have two components in θ- and φ-directions, respectively (Fig. 1). The surface currents

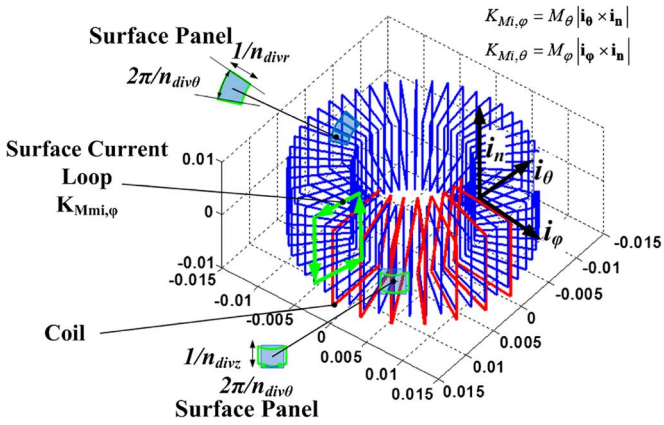

Fig. 1. $K_{mi,\varphi}$ surface magnetic currents and the coil on the toroidal magnetic inductor: $K_{mi,\varphi}$ form rectangular loops, while coil currents form a spiral around the core; mesh is defined by magnetic surface panels and magnetic current loops (arrow).

$\mathbf{K_{M,\varphi}}$ produce the axial flux within the core, whereas the surface currents $\mathbf{K_{M,\theta}}$ originate from the field lines going out of the core. It can be shown that the amplitude of $\mathbf{K_{M,\varphi}}$ currents is a few orders higher than the amplitude of $\mathbf{K_{M,\theta}}$ currents for practical magnetic cores so that $\mathbf{K_{M,\theta}}$ does not have significant influence on the calculation of magnetic field within the core. Accordingly, the increase of the main magnetic flux density within the coil has to be described by means of the magnetic surface currents $\mathbf{K_{M,\varphi}}$, and the external effects, like the stray field, are modeled by means of fictitious magnetic charges in this paper.

Altogether, the magnetic core can be modeled by meshing the core surface into N_M panels carrying the currents $\mathbf{K_{Mi,\varphi}}$ and charges σ_{Mi} $(i = 1 \ldots N_M)$. As a result, the number of unknowns is increased by $2N_M$.

III. PEEC Modeling of Inductors

The geometry of interest is a coil wound around a toroidal magnetic core with a rectangular cross section. The coil with N_J turns is modeled by $4N_J$ cylindrical volume subcells, where a turn is approximated as a PEEC volume cell consisting of four connected cylindrical volume subcells. Thus, in the case of a winding with N_J turns, the number of electrically equivalent PEEC nodes is equal to $N_S = N_J + 1$. PEEC modeling of the magnetic core is based on introducing magnetic surface cells carrying the surface currents $\mathbf{K_{Mi,\varphi}}$ and the charges σ_{Mi} $(i = 1 \ldots N_M)$. The coil and the magnetic currents $\mathbf{K_{Mi,\varphi}}$ are descriptively presented in Fig. 1.

A. Boundary Element Equations

The correlation between the electric currents and the magnetic surface quantities, currents, and charges is derived from the boundary conditions of Maxwell's equations. According to Maxwell's EM theory, the continuity of the tangential component H_t and the normal component B_n have to be satisfied at the interface between two different media. If the magnetic field is derived from the magnetic vector potential, the continuity of B_n is automatically enforced by the definition of $\mathbf{A_M}$ and the continuity of H_t has to be set. For magnetic scalar potential, the opposite conditions are applied respectively. Using both magnetic virtual quantities, the boundary equations concerning H_t

and B_n for the kth magnetic panel ($k = 1 \ldots N_M$) are given by [8]

$$\left(\frac{\mathbf{B_{J(Mk)}}}{\mu_0}+\frac{\mathbf{B_{M(Mk)}}}{\mu_0}\right)\times\mathbf{n_{Mk}}-\left(\frac{1}{2}+\frac{1}{\chi_m}\right)\mathbf{K_{Mk}}=0$$
$$\Rightarrow \boldsymbol{\lambda}_{\mathbf{MI}}\cdot\mathbf{I}+\boldsymbol{\alpha}_{\mathbf{MM1}}\cdot\mathbf{K_M}+\boldsymbol{\alpha}_{\mathbf{MM2}}\cdot\boldsymbol{\sigma}_{\mathbf{M}}=\mathbf{0} \quad (5)$$

$$(\mathbf{H_{J,Mk}}+\mathbf{H_{M,Mk}})\bullet\mathbf{n_{Mk}}-\left(\frac{1}{2}+\frac{1}{\chi_m}\right)\sigma_{Mk}=0$$
$$\Rightarrow \boldsymbol{\lambda}_{\mathbf{qMI}}\cdot\mathbf{I}+\boldsymbol{\gamma}_{\mathbf{MM1}}\cdot K_{\mathbf{M}}+\boldsymbol{\gamma}_{\mathbf{MM2}}\cdot\boldsymbol{\sigma}_{\mathbf{M}}=\mathbf{0} \quad (6)$$

where $\mathbf{n_{Mk}}$ is the unit vector pointing outwards normal to the kth magnetic panel, and $\mathbf{B_{(Mk)}}$ and $\mathbf{H_{(Mk)}}$ are the magnetic induction and the magnetic field strength at the kth magnetic panel produced by the coil and other magnetic panels ($i \neq k$).

The influence of the kth magnetic panel to itself (a singularity calculation problem) is defined by the coefficient α_{Mkk}. As the mesh size has an obvious influence on the final results and the calculated singularity (the term $\alpha_{Mkk} = 1/2$) in (5) does not depend on the panel size, a calculation error arises, and a modification of the α_{Mkk} coefficients is performed by enforcing the cancellation of the permeability-free terms according to [9]. The $\boldsymbol{\alpha}$, $\boldsymbol{\lambda}$, and $\boldsymbol{\gamma}$ matrices provide the additional set of equations needed for solving the PEEC modeling problem extended by $2N_M$ unknowns $[\mathbf{K_{M,\varphi}}, \sigma_M]$. The $\boldsymbol{\alpha}$ and $\boldsymbol{\gamma}$ matrix elements are defined by (7)–(10), which are derived from (1) and (3) observing the magnetic surface panels carrying fictitious constant currents $\mathbf{K_{Mk,\varphi}}$ and charges σ_{Mk} ($k = 1 \ldots N_M$)

$$\alpha_{MM1}(mk,mj) = \left\{\frac{1}{4\pi}\left[\int_{S_{mj}}\frac{\mathbf{f_M(r_{mj})}\times(\mathbf{r_{mk}}-\mathbf{r_{mj}})}{|\mathbf{r_{mk}}-\mathbf{r_{mj}}|^3}\mathrm{d}S_{mj}\right]\times\mathbf{n_{mk}}\right\}\cdot\mathbf{f_M(r_{mk})} \quad (7)$$

$$\alpha_{MM2}(mk,mj) = \left\{\frac{1}{4\pi}\left[\int_{S_{mj}}\frac{(\mathbf{r_{mk}}-\mathbf{r_{mj}})}{|\mathbf{r_{mk}}-\mathbf{r_{mj}}|^3}\mathrm{d}S_{mj}\right]\times\mathbf{n_{mk}}\right\}\cdot\mathbf{f_M(r_{mk})} \quad (8)$$

$$\gamma_{MM1}(mk,mj) = \frac{1}{4\pi}\left[\int_{S_{mj}}\frac{\mathbf{f_M(r_{mj})}\times(\mathbf{r_{mk}}-\mathbf{r_{mj}})}{|\mathbf{r_{mk}}-\mathbf{r_{mj}}|^3}\mathrm{d}S_{mj}\right]\cdot\mathbf{n_{mk}} \quad (9)$$

$$\gamma_{MM1}(mk,mj) = \frac{1}{4\pi}\left[\int_{S_{mj}}\frac{(\mathbf{r_{mk}}-\mathbf{r_{mj}})}{|\mathbf{r_{mk}}-\mathbf{r_{mj}}|^3}\mathrm{d}S_{mj}\right]\cdot\mathbf{n_{mk}} \quad (10)$$

where $\mathbf{r_{mk}}$ is the observation point lying on the mkth magnetic panel, and $\mathbf{f_M(r_{mk})}$ is the tangential unit vector (either i_φ or i_z, see Fig. 1) on the mkth magnetic panel carrying the fictitious surface current $\mathbf{K_{Mk}}$, i.e., $\mathbf{K_{Mk}} = \mathrm{K_{Mk}}\cdot\mathbf{f_M(r_{mk})}$. The matrix entries of $\boldsymbol{\lambda}$ are derived from the Biot–Savart law considering the coil as source of magnetic field. To accelerate the matrix elements calculation of $\boldsymbol{\alpha}$, $\boldsymbol{\lambda}$, and $\boldsymbol{\gamma}$, a filament approach [10] is applied using analytical formulas for the magnetic field of a current carrying arc-conductor and the electric field of uniformly charged circular arc.

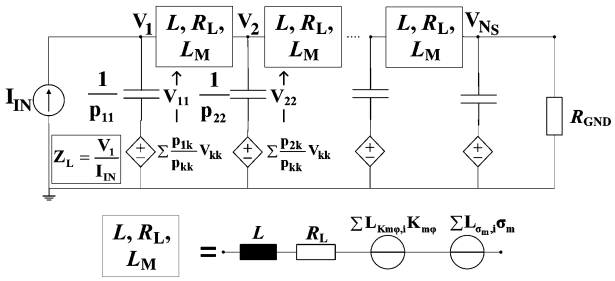

Fig. 2. PEEC equivalent circuit for a magnetic inductor.

B. Coupling PEEC and Boundary Element Methods

Through replacing the core with magnetic surface currents and charges, it is possible to modify the electric field integral equations (EFIE), keeping the structure of the PEEC equations suitable for a circuit description. If the kth electric PEEC volume cell, i.e., kth turn ($k = 1 \ldots N_J$), is observed, the ordinary PEEC EFIE can be rewritten as

$$V_k = R_k I_k + \sum_{i=1}^{N_J} L_{ik}\frac{dI_i}{dt} + \sum_{i=1}^{N_S} P_{ik}Q_i + \sum_{mi=1}^{N_M} L_{Kmi,k}\frac{dK_{mi}}{dt} + L_{\sigma mi,k}\frac{d\sigma_{mi}}{dt}. \quad (11)$$

The EFIE is extended by the matrices $\mathbf{L_{Km}}$ and $\mathbf{L_{\sigma M}}$ consisting of additional partial elements defining the mutual coupling of the fictitious surface magnetic currents $\mathbf{K_{Mk}}$ and charges σ_{Mk} ($k = 1 \ldots N_M$) with the winding currents $\mathbf{I_i}$ ($i = 1 \ldots N_J$). The elements of the matrix $\mathbf{L_{Km}}$ are calculated according to the formula for mutual inductance between two current filaments [10], while the elements of $\mathbf{L_{\sigma M}}$ are calculated according to the approach presented in [11].

The standard PEEC system matrix [2] is extended and takes the form of (12), where $\mathbf{L_M} = [\mathbf{L_{Km}}, \mathbf{L_{\sigma M}}]$, $\boldsymbol{\alpha}_{\mathbf{MM}} = [\boldsymbol{\alpha}_{\mathbf{MM1}}, \boldsymbol{\alpha}_{\mathbf{MM2}}]$, $\boldsymbol{\gamma}_{\mathbf{MM}} = [\boldsymbol{\gamma}_{\mathbf{MM1}}, \boldsymbol{\gamma}_{\mathbf{MM2}}]$, and $\mathbf{A}$ is an $N_J \times N_S$ connectivity matrix. The coefficients of potential matrix $\mathbf{P}$ contain the turn–turn winding capacitance. An illustration of the used PEEC basic cells for modeling the toroidal inductor is presented in Fig. 2

$$\begin{bmatrix}\mathbf{A} & -(\mathbf{R}+j\omega\mathbf{L}) & -j\omega\mathbf{L_M}\\ (j\omega\mathbf{P^{-1}}+\mathbf{Y_L}) & \mathbf{A}^T & 0\\ 0 & \boldsymbol{\lambda}_{\mathbf{MI}} & \boldsymbol{\alpha}_{\mathbf{MM}}\\ 0 & \boldsymbol{\lambda}_{\mathbf{qMI}} & \boldsymbol{\gamma}_{\mathbf{MM}}\end{bmatrix}\begin{bmatrix}\mathbf{V}\\ \mathbf{I}\\ \mathbf{K_M}\\ \boldsymbol{\sigma}_{\mathbf{M}}\end{bmatrix}=\begin{bmatrix}\mathbf{V_S}\\ \mathbf{I_S}\\ \mathbf{0}\\ \mathbf{0}\end{bmatrix} \quad (12)$$

IV. PEEC Simulation and Comparison to Measurements

To verify the proposed PEEC model of a toroidal magnetic inductor, the impedance measurements for several different winding arrangements and core materials were performed using an Agilent 4294A impedance analyzer in the frequency range from 40 Hz up to 110 MHz. The input parameters of the PEEC simulation are the winding arrangements (number of turns, uniform/nonuniform winding, distance between core and winding), the core dimensions (height, inner and outer diameter), and the core magnetic properties (complex permeability or the effective relative permeability curves). The performance of the PEEC simulation is illustrated on the example of two EPCOS ferrite T38 inductors with 3 and 20 turns, respectively

TABLE I
INFORMATION ABOUT THE SELECTED MAGNETIC INDUCTORS

Exp.	Manufacturer	Core Material/Dimensions/	Winding Arrangement [a] / No. Turns / Wire Diam.
1	EPCOS	Ferrite T38 / R 34	NU / 3 / 1.5mm
2	EPCOS	Ferrite T38 / R 34	NU / 20 / 1.5mm

[a] U—uniform/NU—nonuniform winding arrangement along core.

(see Table I). The simulation time for the impedance characteristics in 200 frequency steps is approximately 2 min (on a standard PC) depending on the mesh size and the number of turns.

A. Simulation Parameters and Mesh

The critical input parameter for the PEEC simulation is the permeability characteristics of the core material. For ferrites characterized by higher relative permittivity $\varepsilon(=\ \varepsilon' - \mathrm{j}\varepsilon'')$, the manufacturers measure permeability characteristics on small ring cores, e.g., R10, to avoid dimensional effects [12]. Accordingly, the permeability curves from datasheets do not correctly describe the intrinsic permeability of cores with different dimensions. The second problem is a material variation from core to core, i.e., data provided by manufacturers could deviate from the actual behavior by 20%–30%, and the permeability characteristics can only be statistically determined by measuring several cores with the same dimensions. In addition, the winding arrangement can significantly alter permeability measurement results at higher frequencies, so special care must be taken concerning the number of turns and the winding arrangement. Namely, the standard inductance measurements do not provide information only about the permeability properties of the material, but contain the influence of winding and/or dimensional effects at higher frequencies.

B. PEEC Simulation Results

The mesh of the magnetic surface is defined by the discretization in θ-, z-, and r-directions, respectively, $n_{\mathrm{div}\theta}$, $n_{\mathrm{div}z}$, and $n_{\mathrm{div}r}$ (Fig. 1). Analyzing the terms in (11), we observed that the calculation of impedance is primarily determined by the magnetic currents $\mathbf{K}_{\mathrm{M},\varphi}$, which in turn do not produce a significant influence on the field outside when $n_{\mathrm{div}\theta}$ is sufficiently high.

An inductor with three turns exhibiting low influence of windings is used for the complex permeability measurements, and a 20-turns inductor with identical core is used for the model verification. From the measured permeability characteristics in Fig. 3 (left), it can be seen that the real permeability decreases and becomes negative for $f_1 \approx 2$ MHz. This implies that the inductor with only three turns becomes capacitive in the low-loss frequency range, which can be ascribed to high core permittivity, $\varepsilon \approx 2 \cdot 10^5$. The simulation results of the 20-turns inductor are presented in Fig. 3 (right). The simulation results comply with the measurements in the frequency range up to f_1. Above f_1, the simulation does not match the measurements as the input permeability curves do not provide accurate information about the intrinsic magnetic properties of the core. Hence, to achieve better simulation results at higher frequencies, both complex permeability and permittivity measurements need to be performed [13]. Further steps will be to include the core permittivity ε as a simulation parameter (turn-to-core capacitance).

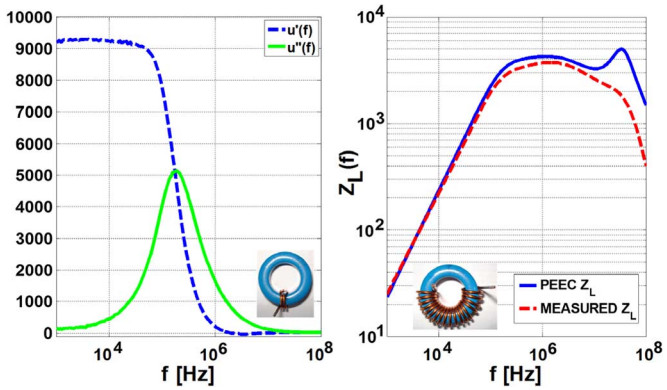

Fig. 3. *(left)* Measured complex permeability for EPCOS ferrite T38 R 34 ring core (see Table I). Real part (dashed line) and imaginary part (solid line). *(right)* Comparison of the impedance of the PEEC modeled inductor with the measurement (Ferrite T38 R 34—20 turns).

REFERENCES

[1] J. Ekman and G. Antonini, "On characterizing artifacts observed in PEEC based modeling," in *Proc. IEEE EMC*, Santa Clara, CA, Aug. 9–13, 2004, pp. 251–255.
[2] G. Antonini, M. Sabatini, and G. Miscione, "PEEC modeling of linear magnetic materials," in *Proc. IEEE EMC*, Portland, OR, Aug. 14–18, 2006, pp. 93–98.
[3] J. P. Keradec, E. Clavel, J. P. Gonnet, and V. Mazauric, "Introducing linear magnetic materials in PEEC simulations. Principles, academic and industrial applications," in *Proc. 40th Ind. Appl. Conf.*, Hong Kong, Oct. 2–6, 2005, pp. 2236–2240.
[4] H. Long, Z. Feng, H. Feng, and A. Wang, "A novel accurate PEEC-based 3D modeling technique for RF devices of arbitrary conductor-magnet structure," *Microw. Opt. Technol. Lett.*, vol. 38, no. 3, pp. 237–240, Jun. 2003.
[5] E. Hoene, A. Lissner, S. Weber, S. Guttowski, W. John, and H. Reichl, "Simulating electromagnetic interactions in high power density converters," in *Proc. 36th Power Electron. Specialists Conf.*, Recife, Brazil, Jun. 12–16, 2005, pp. 1665–1670.
[6] T. S. Tran, G. Meunier, P. Labie, Y. Le Floch, J. Roudet, J. M. Guichon, and Y. Marechal, "Coupling PEEC-finite element method for solving electromagnetic problems," *IEEE Trans. Magn.*, vol. 44, no. 6, pp. 1330–1333, Jun. 2008.
[7] D. M. Cook, *The Theory of the Electromagnetic Field*. Englewood Cliffs, NJ: Prentice-Hall, 1975, pp. 289–324.
[8] A. Nicolet, "Boundary elements and singular integrals in 3D magnetostatics," *Eng. Anal. Boundary Elements*, vol. 13, no. 2, pp. 193–200, 1994.
[9] T. Morisue, "3-D magnetostatic field calculation for a magnetic circuit with no (a narrow) air gap," *IEEE Trans. Magn.*, vol. 25, no. 5, pp. 3266–3268, Nov. 1989.
[10] A. Musing, J. Ekman, and J. W. Kolar, "Efficient calculation of non-orthogonal partial elements for the PEEC method," *IEEE Trans. Magn.*, vol. 45, no. 3, pp. 1140–43, Mar. 2009.
[11] Y. Massoud and J. Whyte, "Improving the generality of the fictitious magnetic charge approach to computing inductance in the presence of permeable material," in *Proc. 39th Annu. Design Autom. Conf.*, New Orleans, LA, Jun. 10–14, 2002, pp. 552–555.
[12] R. Huang and D. Zhang, "Experimentally verified Mn-Zn ferrites intrinsic complex permittivity and permeability tracing technique using two ferrite capacitors," *IEEE Trans. Magn.*, vol. 43, no. 3, pp. 974–981, Mar. 2007.
[13] J. P. Keredec, P. Fouassier, B. Cogitore, and F. Blache, "Accounting for resistivity and permittivity in high frequency permeability measurements application to MnZn ferrites," in *Proc 20th IMTC*, Vail, CO, May 20–22, 2003, vol. 2, pp. 1252–1256.